V18

Germanium detector in gamma spectroscopy

Christopher Breitfeld
christopher.breitfeld@tu-dortmund.de

Henry Krämerkämper
henry.kraemerkaemper@tu-dortmund.de

Conducted : 20. November 2023 Submission: February 14, 2024

TU Dortmund – Fakultät Physik

Contents

1 Aims of the Experiment

Goal of the experiment is to examine energy and activity of radioactive sources. To achieve this, the spectra of this sources are measured with a germanium detector.

2 Theory

2.1 Interaction of γ Photons with Matter

The intensity of a γ photon in a material, dependent on the penetration depth x, is described by the Lambert-Beer law

$$I(x) = I_0 \exp(-\mu x) \tag{1}$$

where I_0 describes the primary intensity of the γ photon. μ is the extinction coefficient, dependent on the atomic number Z, the particle number density n, and the cross-section σ of the process

$$\mu = Zn\sigma. \tag{2}$$

The interaction of photons with matter depends on the photon's energy and is therefore distinguished into three different processes for γ photons, each with different cross-sections.

Photoelectric Effect

The photoelectric effect (photoeffect) is a process in which the photon interacts with a valence electron of an atom. If the energy of the photon is greater than the work function with which the electron is bound to the atom, the electron leaves the atom. The photon is thereby fully absorbed. The hole created by this process is filled up with electrons from higher energy levels, leading to the emission of new photons. Usually, all photons stay inside the material, so that the energy of the initial photon is fully absorbed.
The cross-section of this process not only depends on the energy but also on the material. Specifically, the cross-section is given by

$$\sigma_{\text{Photo}} \approx 3 \cdot 10^{12} Z^{\alpha} E_{\gamma}^{\delta} \tag{3}$$

with $3 < \alpha < 4$ and $\delta \approx -3$.

Compton Scattering

Compton scattering is the inelastic scattering of γ photons with quasi-free electrons. During this process, the photon transfers a portion of its energy to the electron, resulting in a change in its wavelength. This phenomenon is described by

$$\lambda' = \lambda + \lambda_{\text{Compton}}(1 - \cos\theta) \tag{4}$$

where λ is the initial wavelength, λ' is the wavelength afterward, and $\lambda_{\text{Compton}} = h/(m_e c)$ is the Compton wavelength. The energy transfer depends on the scattering angle θ, with maximum energy transfer occurring at $\theta = \pi$.

The cross-section is given by the Klein-Nishina equation

$$\sigma_{\text{Compton}} = \frac{\pi\alpha^2}{m^2}\frac{1}{\hat{E}^3}\left(\frac{2\hat{E}(2+\hat{E}(1+\hat{E})(8+\hat{E}))}{(1+2\hat{E})^2} + ((\hat{E}-2)\hat{E}-2)\log(1+2\hat{E})\right) \tag{5}$$

with the normalized energy $\hat{E} = E'/E = \lambda/\lambda'$.

2.1.1 Pair Production

If the energy of the photon exceeds twice the electron mass, pair production becomes relevant. Although free photon decay $\gamma \rightarrow e^+e^-$ is forbidden due to the photon's masslessness, when interacting with an atom, the photon can produce an electron-positron pair by transferring momentum to the atom. The cross-section depends on the potential shielding and the atomic number Z

$$\sigma_{\text{Pair}} \propto \alpha Z^2 \tag{6}$$

Figure 1 illustrates the contribution of the discussed processes to the total extinction coefficient as a function of energy. The photoelectric effect dominates at lower energies, pair production prevails in the high-energy range, and Compton scattering provides significant contributions in between.

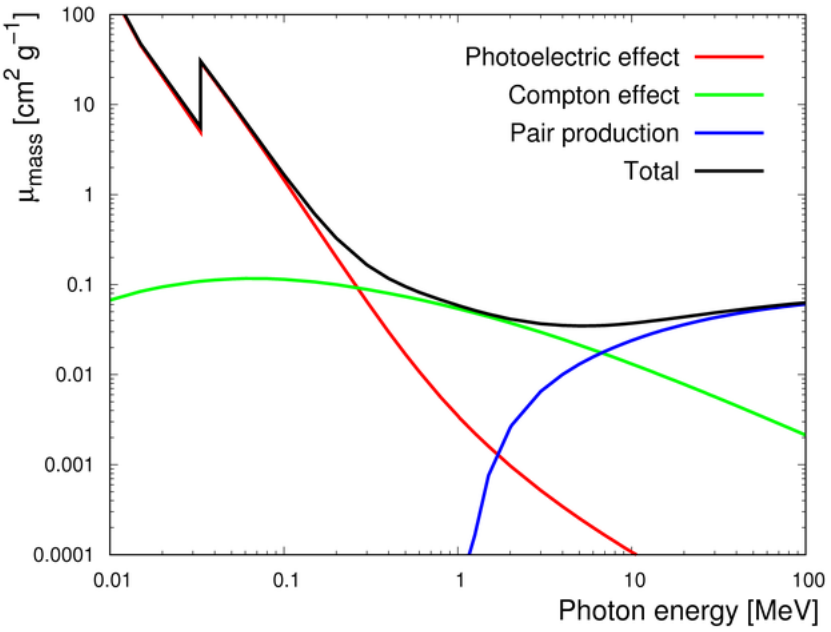

Figure 1: Influence of the photoelectric effect, Compton scattering and pair production on the extinction coefficient as a function of energy [4].

2.2 Function of a Semiconductor Detector

A semiconductor is a material with a valence and conduction band separated by a small band gap. At low temperatures, the valence band is fully occupied with electrons, while the conduction band remains empty. At higher temperatures, electrons can transition to the conduction band, leaving a hole in the valence band.
Additionally, the semiconductor can be doped with atoms that introduce more or fewer valence electrons than the semiconductor. If the doping atom has fewer valence electrons, it creates an additional hole, resulting in a positively (p) doped material. Conversely, if the doping atom introduces more electrons, it leads to a negatively (n) doped material.
A semiconductor detector essentially functions as a diode, where n and p doped regions border each other. The interface between these regions has fewer charge carriers due to recombination between the carriers from the n and p doped zones, creating a depletion zone. Recombination continues until the electric field of the remaining charges establishes equilibrium. The extent of the depletion zone can be expanded by applying an electric field.
When a γ photon is incident, it generates a high-energy electron through a process described in Section 2.1. This energetic electron imparts its energy to other electrons in the semiconductor, causing them to jump from the valence to the conduction band. Consequently, a γ photon creates multiple electrons and holes within the depletion zone. The electric field separates these charge carriers before they can recombine. The resulting charge pulse constitutes the measured signal. Thus the signal intensity increases with the energy of the incoming γ photon.
Figure 2 depicts the schematic structure of a semiconductor detector.

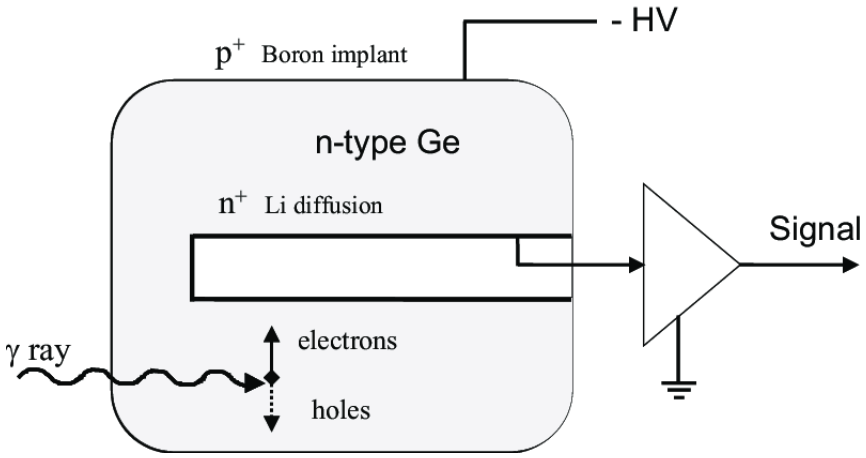

Figure 2: Schematic illustration of a germanium detector [3].

2.3 Expected Spectrum of a Monochromatic γ Source

The number of counts N measured with a germanium detector, when a small γ source is placed next to it, depends on the emission probability P of the source, the activity A,

the distance between the source and the detector (thus the solid angle component Ω), and the time t. It is given by

$$N_{\text{theory}} = P \cdot \frac{\Omega}{4\pi} \cdot A \cdot t. \tag{7}$$

If the source is monochromatic, meaning that all γ photons have the same energy, the spectrum of the number of counts in dependence on the energy exhibits distinct peaks. Figure 3 illustrates the expected spectrum of a monochromatic source, consisting of the photopeak, the Compton edge, and a backscattering peak in the Compton continuum. The photopeak occurs at the energy of the γ photon, as the entire energy of the photon is absorbed in the photoeffect. Below the photopeak lies the Compton continuum, with its maximum at the Compton edge where the scattering angle is $\theta = \pi$. Lower energies correspond to other scattering angles. Within the Compton continuum lies the backscattering peak, resulting from gammas undergoing Compton scattering outside the detector but backscattering into the detector before being fully absorbed. The effect of pair production is not relevant for the sources used in this experiment.

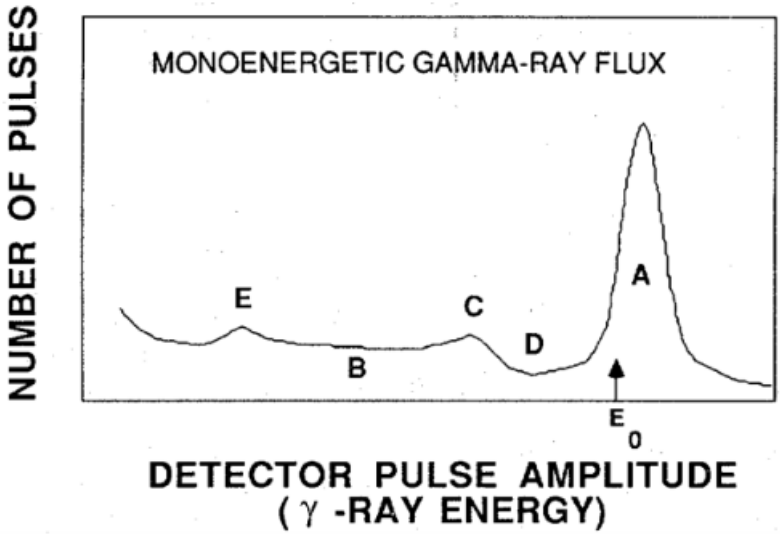

Figure 3: Spectrum of a monochromatic γ source with the photopeak (A), the Compton continuum (B), the Compton edge (C), and the backscattering peak (E) [5].

3 Experimental Setup and Measurements

A germanium detector, as depicted in Figure 2, and a radioactive source are placed inside a lead case, which provides shielding.
Each measurement lasts for 45 min. For detector calibration, a sample of ^{152}Eu with well known activity is measured.
After the calibration, the spectra of ^{137}Cs and ^{60}Co samples are measured. Additionally, the spectrum of an unknown sample is measured.

To estimate background radiation during the measurements, a measurement without any sample is conducted over 24 h.

4 Analysis

4.1 Detector Calibration

To calibrate the germanium detector, the spectrum of an ^{152}Eu source is measured; this can be seen in Figure 4. A background measurement is conducted and removed from the ^{152}Eu measurement. For this, the background measurement is scaled according to the difference in measurement time compared to the ^{152}Eu measurement. The background can be seen in Figure 5 and the scaled background as well as the ^{152}Eu measurement in Figure 6. To calibrate the germanium detector, an energy is assigned to each detector

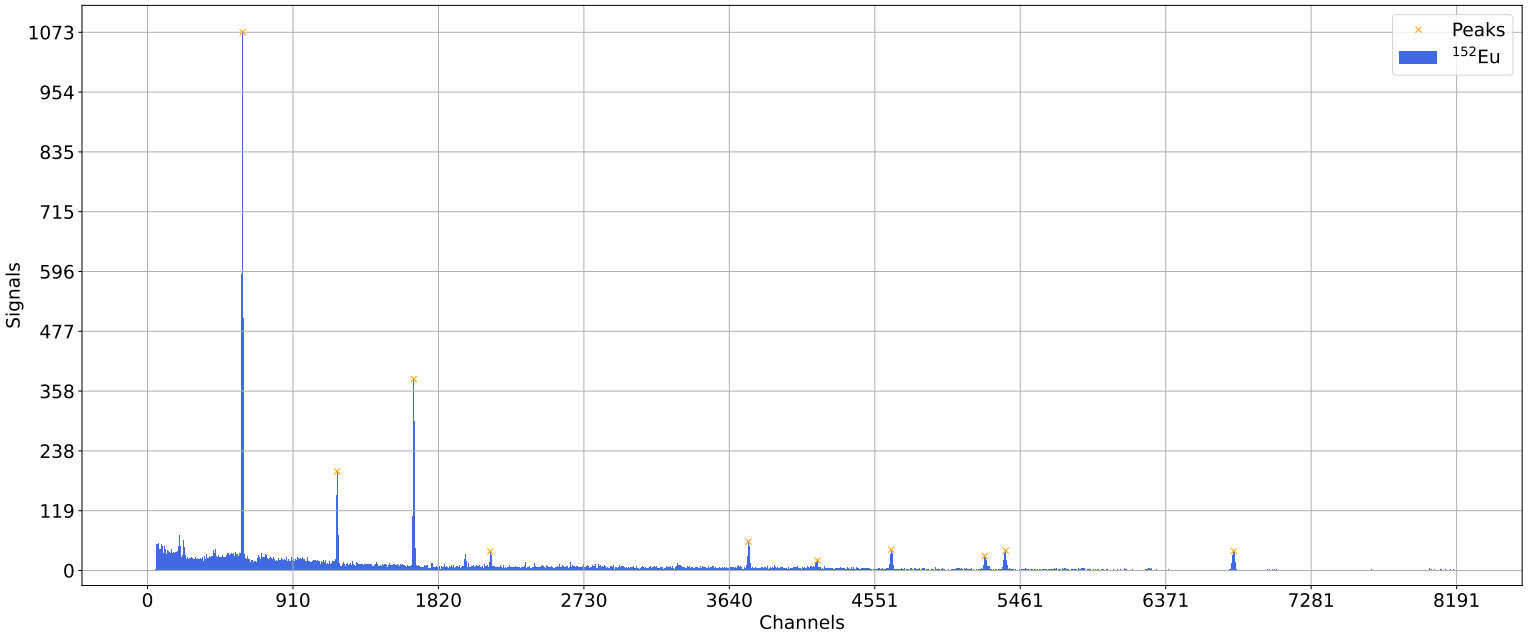

Figure 4: Spectrum of an ^{152}Eu source and its most prominent peaks.

channel. The 10 most prominent full energy peaks are selected and compared to the 10 most probable emission lines of the known ^{152}Eu spectrum [1]. The most prominent full energy peaks are marked in orange in Figure 4 and given in Table 1. The prominence calculation is performed using the algorithm `find_peaks` from the python library `scipy` [6]. A linear fit

$$E(K) = \alpha \cdot K + \beta \tag{8}$$

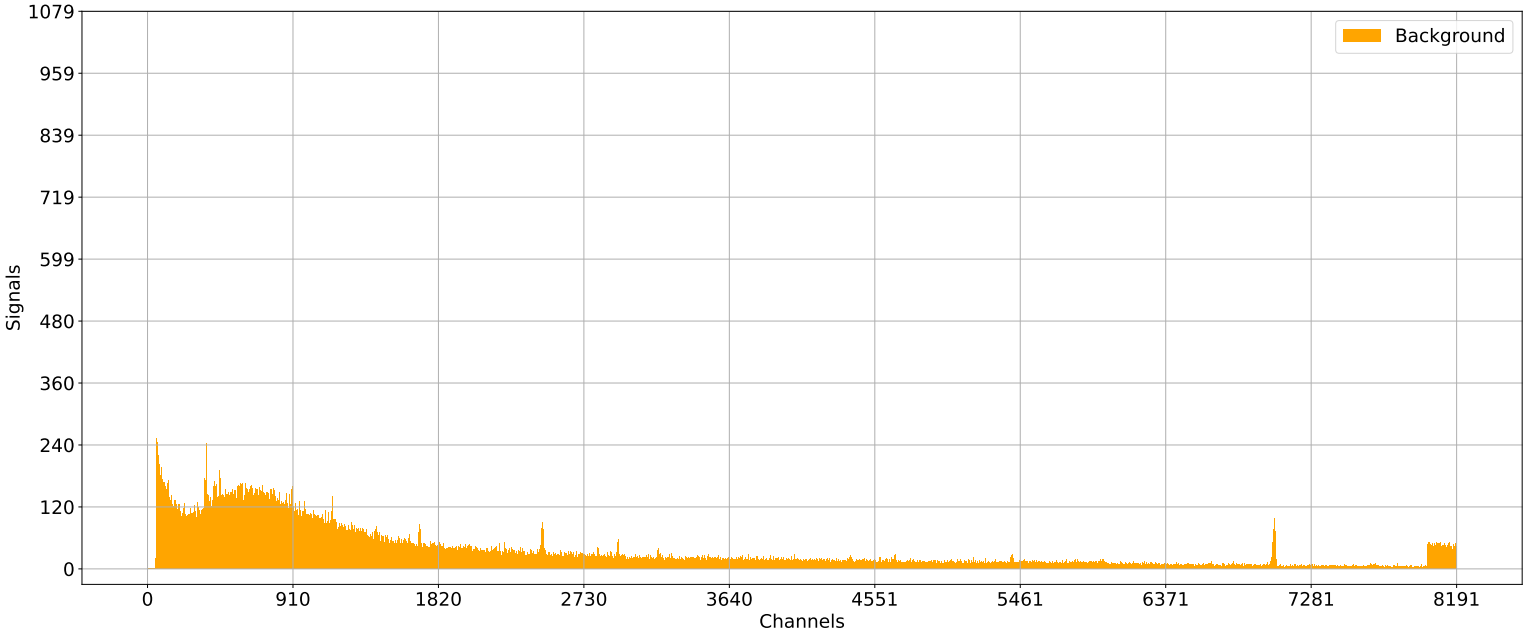

Figure 5: Spectrum of background radiation.

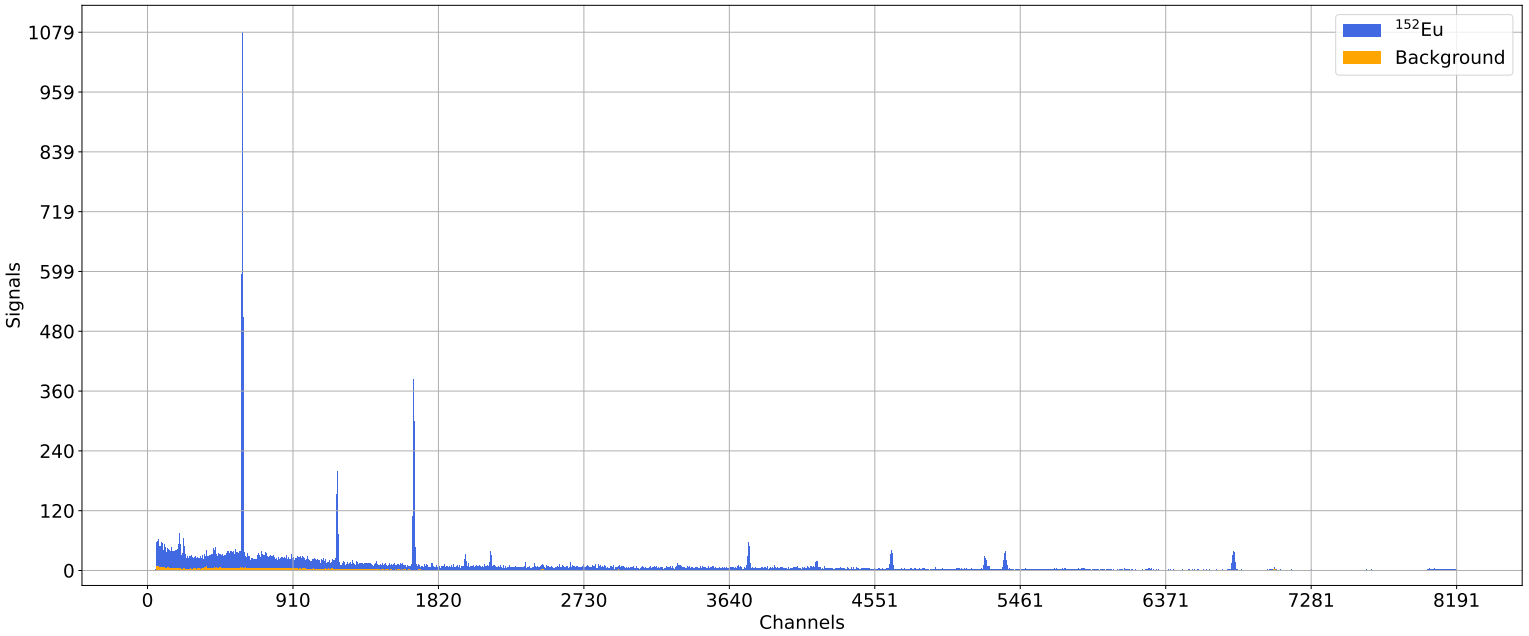

Figure 6: ^{152}Eu measurement and scaled spectrum of background radiation.

is performed to get a relation between energy E and channel number K. The resulting fit parameters are

$$\alpha = 0.2075$$
$$\beta = -1.6225 \pm 0.0004.$$

The fit is displayed in Figure 9. The relation (8) with the determined parameters is used throughout this analysis for energy measurements. The fit is performed using the `iminuit` [2] python package.

Table 1: Energy and emission probability [1] of the full energy peaks, their assigned channel number as well as the yield of each peak, determined by a fit.

E_{lit}/keV	P_{lit}/%	C	N
121.7817	28.41 ±0.13	595	8479 ±103
244.6974	7.55 ±0.04	1187	1597 ±40
344.2785	26.59 ±0.12	1666	3301 ±60
443.9650	2.80 ±0.02	2145	424 ±25
778.9045	12.97 ±0.06	3760	752 ±29
867.3800	4.24 ±0.02	4192	247 ±25
964.0790	14.50 ±0.06	4654	621 ±26
1085.8370	10.13 ±0.06	5238	470 ±39
1112.0760	13.41 ±0.06	5370	586 ±36
1408.0130	20.85 ±0.08	6797	627 ±26

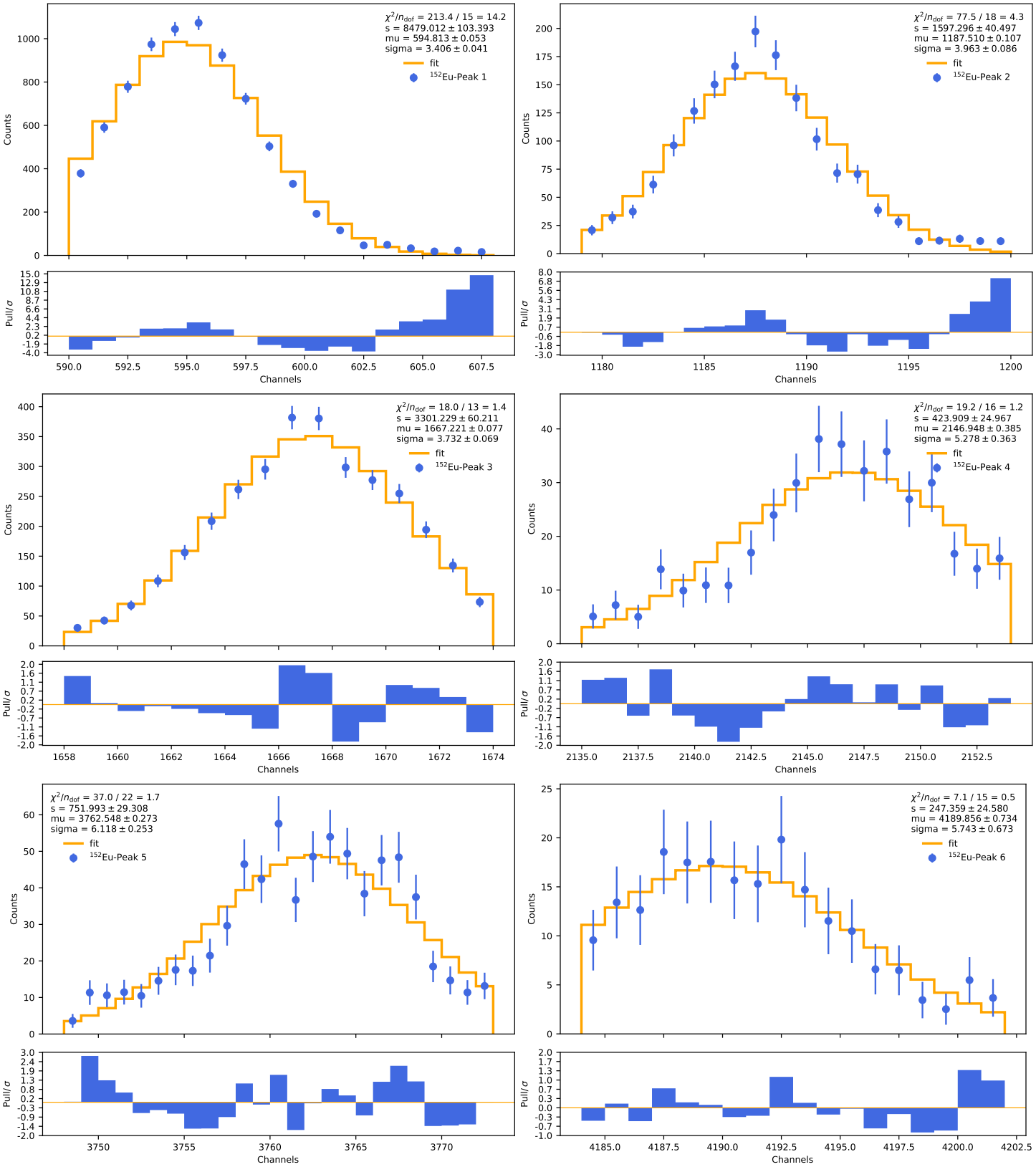

Figure 7: Fits of peaks of the ^{152}Eu spectrum.

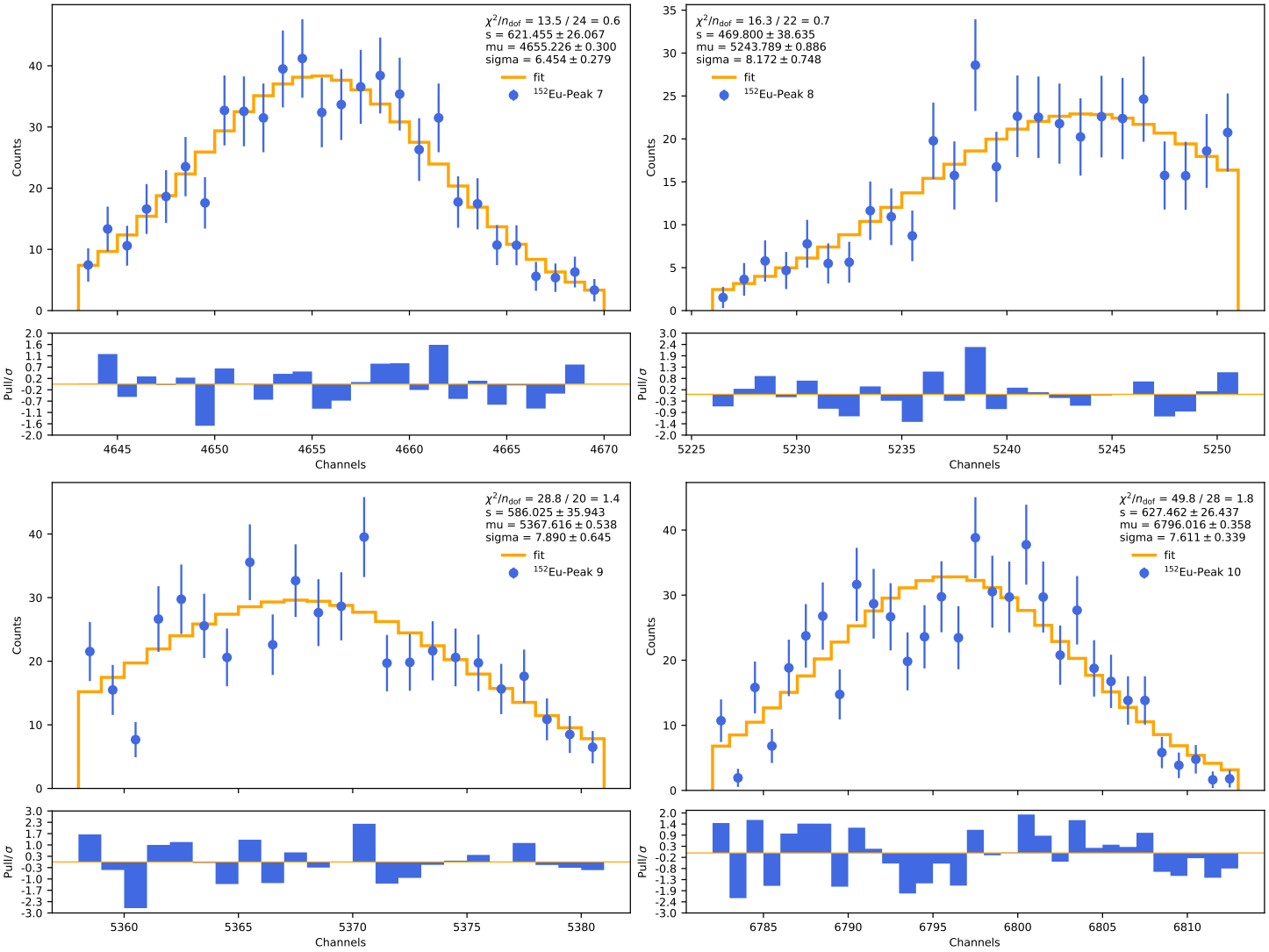

Figure 8: Fits of the 10 most prominent peaks of the ^{152}Eu spectrum.

4.2 The full energy detection probability

The amount of photons which fully penetrate and are registered by the detector is called the full energy detection probability Q. It is given by

$$Q = \frac{4\pi}{\Omega}\frac{N}{APt}. \tag{9}$$

Q depends on the activity of the source A, the emission probability P, the number of measured photons N and the measurement time t. N and P are given in Table 1. Ω is the solid angle covered by the detector. For the germanium detector, Ω is given by

$$\frac{\Omega}{4\pi} = \frac{1}{2}\left(1 - \frac{a}{\sqrt{a^2 + r^2}}\right) \tag{10}$$

with the detectors radius r and the distance to the probe a.

4.2.1 Determination of the probe activity

To determine the full energy detection probability, first the activation of the ^{152}Eu source has to be estimated. The source had an activation of $A_0 = (4130 \pm 60)\,\mathrm{Bq}$ on the 1.10.2000. According to the law of radioactive decay,

$$A(t) = A_0 \cdot \exp\left(-\frac{\ln(2)}{\tau} \cdot t\right) \tag{11}$$

with elapsed time t and half life $\tau = 13.522\,\mathrm{years}$ [1], the activation on the day of the measurement of ^{152}Eu amounts to $A(t_\mathrm{M}) = (1262 \pm 18)\,\mathrm{Bq}$.

4.2.2 Determination of the solid angle

The solid angle $\frac{\Omega}{4\pi}$ covered by the germanium detector is given by equation (10). The detector cylinder has a width of 4.5 cm. The source is located 6.91 cm away from the aluminum cover; the cover itself is 1.5 cm away from the detector. Therefore, the parameters in equation (10) are given by

$$r = 2.25\,\mathrm{cm} \tag{12}$$

$$a = 8.91\,\mathrm{cm}. \tag{13}$$

Using equation (10) and the parameters (13) the solid angle amounts to

$$\frac{\Omega}{4\pi} = 0.01522. \tag{14}$$

4.2.3 Determination of the full energy detection probability

The estimation of the full energy detection probability is performed for all measured spectral lines.

Table 2: Energy and the calculated full energy detection probability of the 12 peaks of the ^{152}Eu spectrum with more than 150 keV.

E/keV	Q/%
121.7817 ±0.0003	0.0555 ±0.0011
244.6974 ±0.0008	0.0393 ±0.0012
344.2785 ±0.0012	0.0231 ±0.0006
443.965 ±0.003	0.0281 ±0.0017
778.9045 ±0.0024	0.0108 ±0.0005
867.38 ±0.003	0.0108 ±0.0011
964.079 ±0.018	0.0080 ±0.0004
1085.837 ±0.01	0.0086 ±0.0007
1112.076 ±0.003	0.0081 ±0.0005
1408.013 ±0.003	0.0056 ±0.0003

To obtain the energy dependency of full energy detection probability, a fit using the function

$$Q(E) = a \cdot E^b \tag{15}$$

is performed for all measured spectral lines with more than 150 keV, which is the limit of the detector sensitivity. The result is displayed in Figure 9.

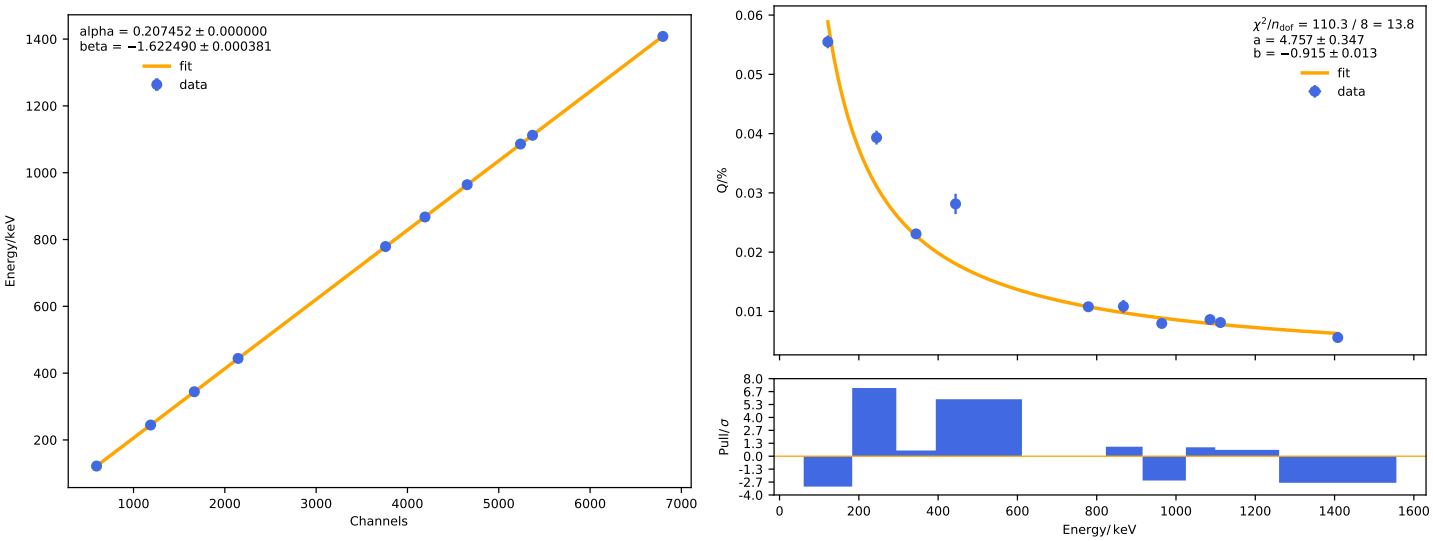

Figure 9: The fit of the measured energy and the detector channels as well as the Fit of the full energy detection probabilities for different peaks of the ^{152}Eu spectrum.

The resulting fit parameters are

$$a = 4.76 \pm 0.35$$
$$b = -0.915 \pm 0.013.$$

The relation (15) with the determined parameters is used to estimate the full energy detection probability throughout this analysis.

4.3 Gamma spectrum of ^{137}Cs

A ^{137}Cs probe was measured as well. The measurement was carried out for $t = 2865$ s. The resulting spectrum is given in Figure 10. The background measurement was again scaled to the appropriate measurement time and then removed. The two peaks marked in Figure 10 are determined using `find_peaks` from the python library `scipy` [6]. A scaled normal distribution is fitted to the peaks using `iminuit` [2] to determine the yield. The results are displayed in Figure 11.

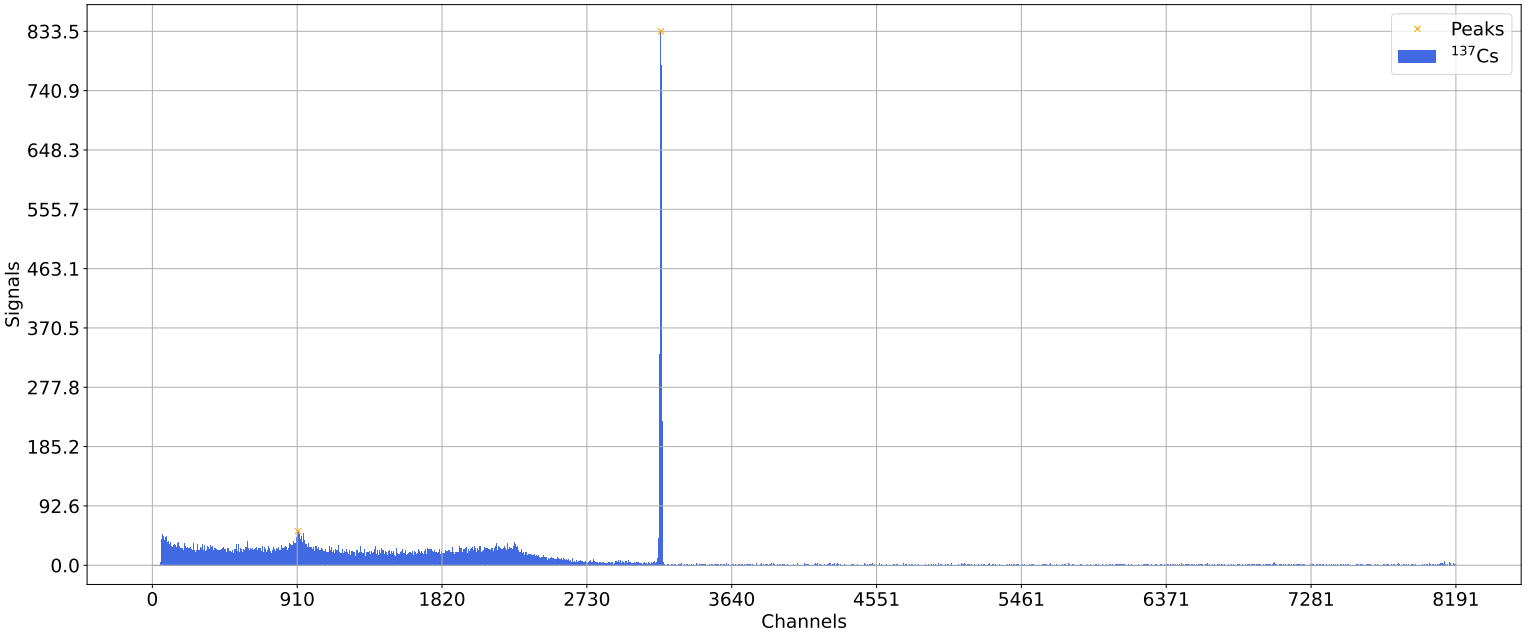

Figure 10: Spectrum of the ^{137}Cs measurement.

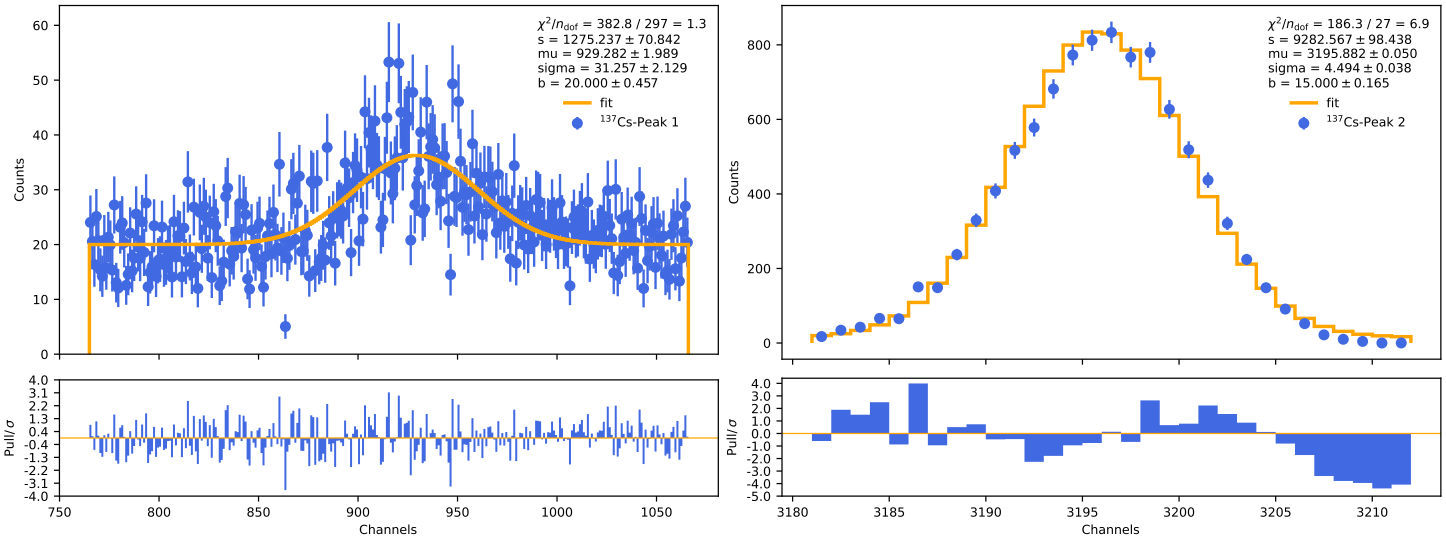

Figure 11: Fits of peaks of the ^{137}Cs spectrum.

These fits include a further background estimation parameter b; the resulting distribution is given in equation (16).

$$g(x) = s \cdot \frac{1}{\sqrt{2\pi}\sigma} \exp\left(-\frac{1}{2}\frac{(x-\mu)^2}{\sigma}\right) + b \tag{16}$$

The fit parameters including the number of events of each peak is given in Table 3; the yield of each peak is given by the scale factor s.

Table 3: Fit parameters of the two peaks of the ^{137}Cs spectrum with more than 150 keV.

E/keV	s	b	μ	σ
188.1961 ±0.0004	1275 ±71	20.00 ±0.46	929.28 ±1.99	31.26 ±2.13
661.3941 ±0.0004	9283 ±98	15.00 ±0.17	3195.88 ±0.05	4.49 ±0.04

The full width at half maximum and full width at tenth maximum of the second peak (which can be identified as the peak caused by the photo effect) of the ^{137}Cs spectrum are estimated. To do this, the fitted normal distribution is utilized. This is displayed in Figure 12. The full width at half maximum and the full width at tenth maximum

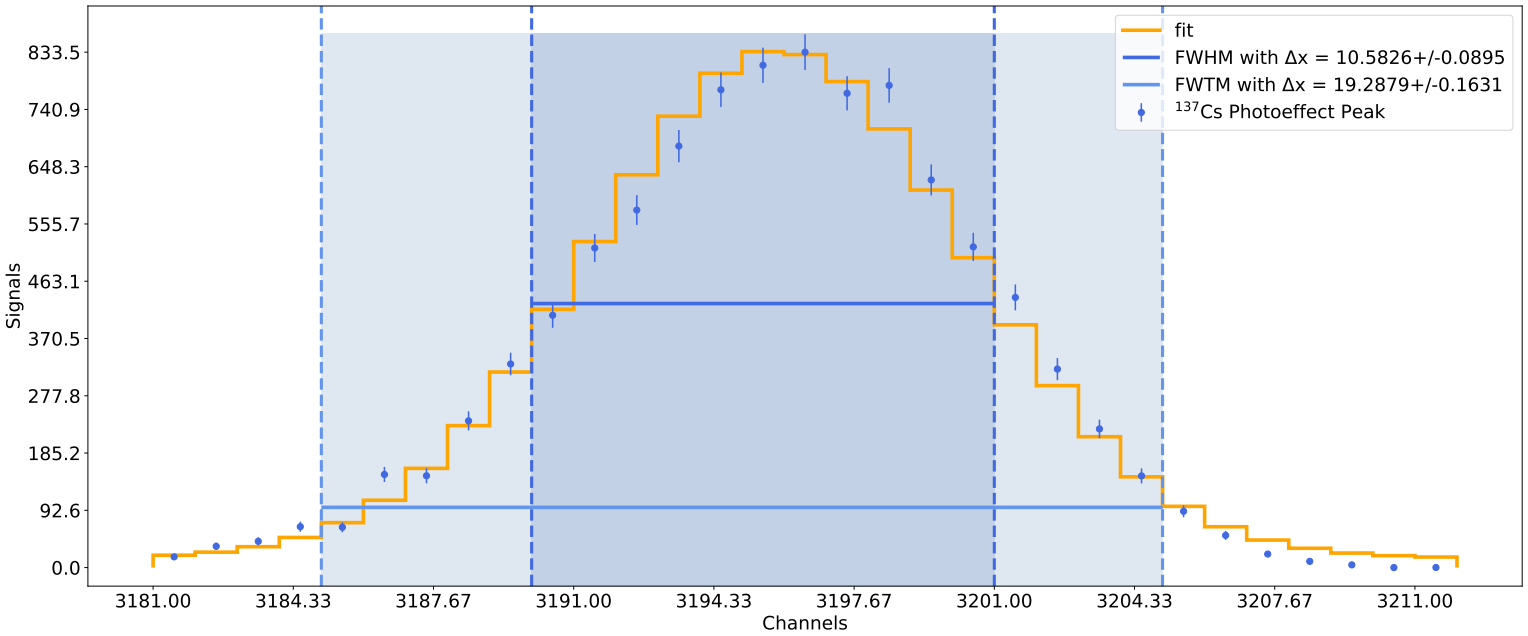

Figure 12: FWHM and FWTM of the photoelectric peak of the ^{137}Cs measurement.

amount to

$$\text{FWHM} = 10.58 \pm 0.09 = (0.573 \pm 0.019)\,\text{keV} \tag{17}$$

$$\text{FWTM} = 19.29 \pm 0.16 = (2.379 \pm 0.034)\,\text{keV}. \tag{18}$$

The ratio of the two is given by

$$\frac{\text{FWHM}}{\text{FWTM}} = 0.5487 = (1.5087 \pm 0.0004)\,\text{keV}. \tag{19}$$

The energy of the photoelectric peak is determined from the fit to

$$E_\gamma = (661.3941 \pm 0.0004)\,\mathrm{keV}. \tag{20}$$

The energy of the compton edge can be calculated using equation (21)

$$E'_\gamma|_{\theta=180°} = \frac{E_\gamma}{1 + \frac{m_e c^2}{2E_\gamma}}. \tag{21}$$

This amounts to

$$E'_\gamma|_{\theta=180°} = (477.0915 \pm 0.0004)\,\mathrm{keV}. \tag{22}$$

The spectrum, including the theoretical value computed above as well as an estimate based on this measurement, is displayed in Figure 13. The compton continuum is estimated and marked in orange. The compton edge is visually estimated to be at $E'_\gamma|_{\theta=180°} = 474.7\,\mathrm{keV}$.

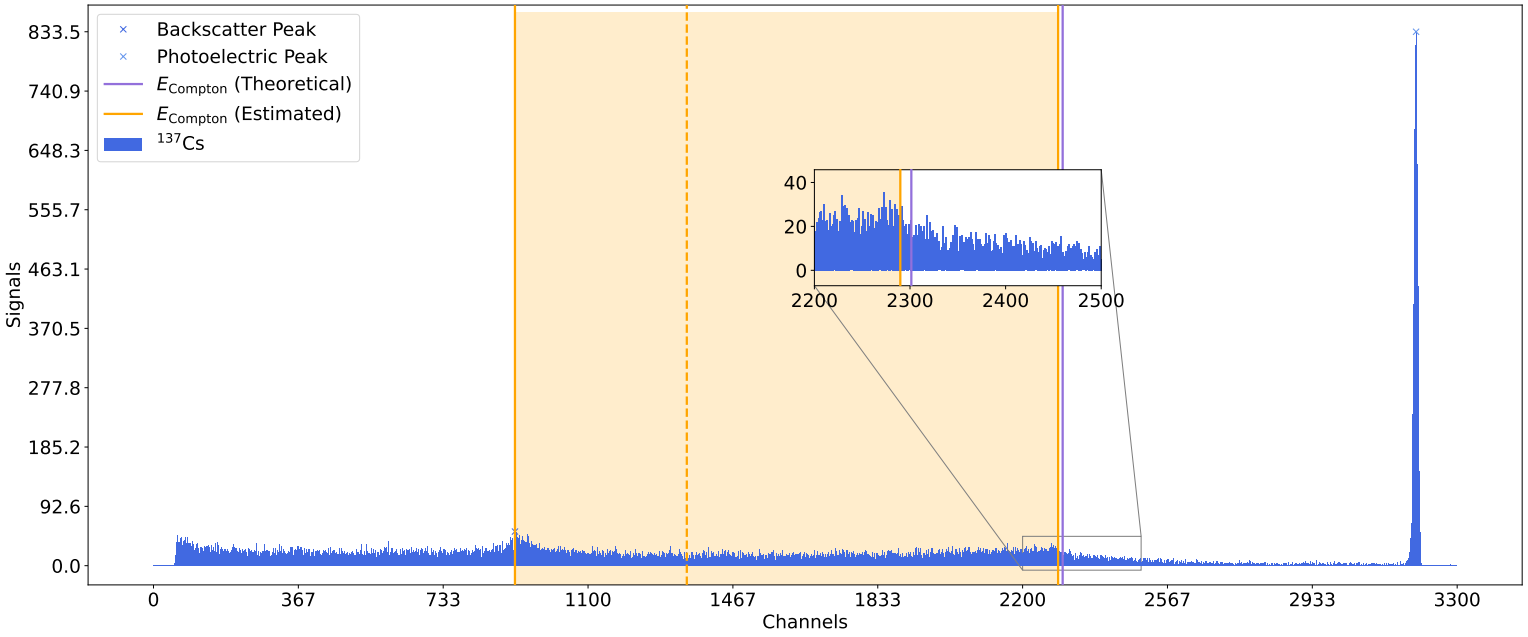

Figure 13: Estimates of the compton edge and continuum of the ^{137}Cs measurement.

The energy region below the compton edge should be dominated by the compton effect and include minimal amounts of background. The backscatter peak is estimated to be at $E_\gamma = (188.1961 \pm 0.0004)\,\mathrm{keV}$. To estimate the event count in the compton continuum, a linear fit is carried out in the region between the backscatter peak and the compton edge. To reduce the influence of the backscatter peak only a certain region from 278.438 keV (marked in Figure 13 as a dashed line) up to the compton edge (at 474.7 keV) is used. The fit is displayed in Figure 14.

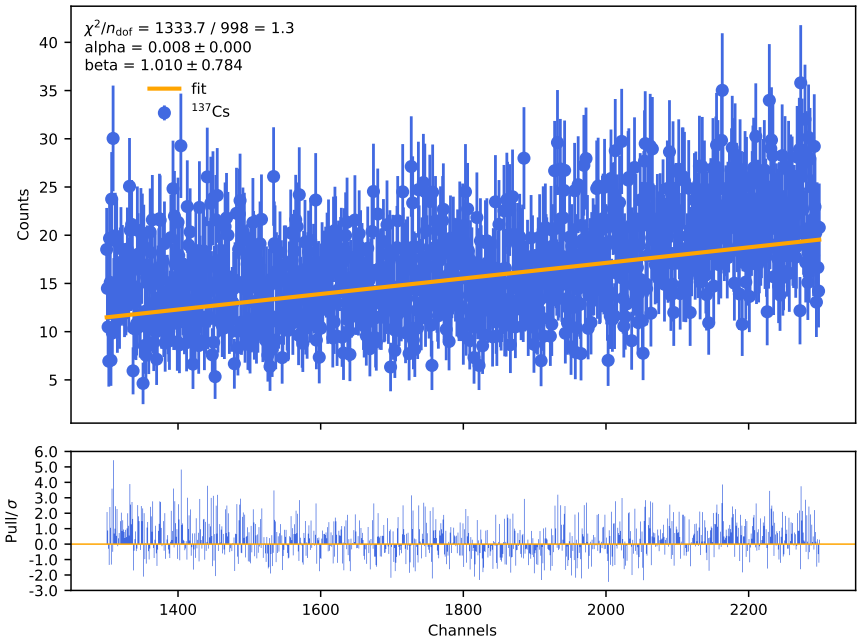

Figure 14: Linear Fit of the compton continuum.

The function utilized here is given in Equation (23)

$$f(x) = \alpha \cdot x + \beta. \tag{23}$$

The parameters are estimated to the values

$$\alpha = 0.008 \tag{24}$$
$$\beta = 1.0 \pm 0.8. \tag{25}$$

This yield of the compton continuum as estimated by this fit amounts to

$$N = 15\,498.848\,30. \tag{26}$$

4.4 Gamma spectrum of ^{60}Co

A measurement of the spectrum of a cobalt probe was conducted for a total measurement time of $t = 4021\,\mathrm{s}$. Again, the background measurement is subtracted. The algorithm `find_peaks` from the python library `scipy` [6] is utilized to determine the exact positions of the peaks. The result is displayed in Figure 15. A comparison to literature values allows the probe to be identified as ^{60}Co [1]. To determine the amount of events belonging to each peak, a fit of the form (27) is carried out.

$$g(x) = s \cdot \frac{1}{\sqrt{2\pi}\sigma} \exp\left(-\frac{1}{2}\frac{(x-\mu)^2}{\sigma}\right) + b \tag{27}$$

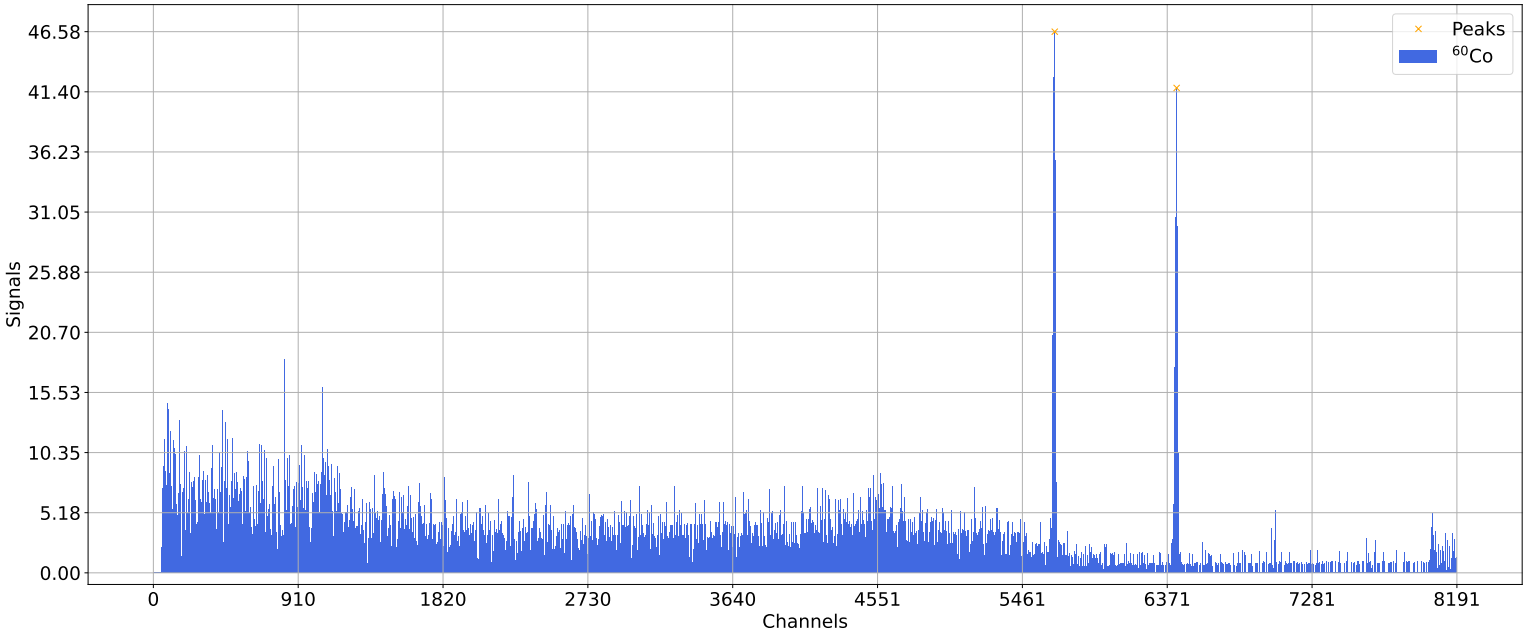

Figure 15: Spectrum of the ^{60}Co measurement.

The results are displayed in Figure 16 and the parameters as well as the peak yields are given in Table 4.

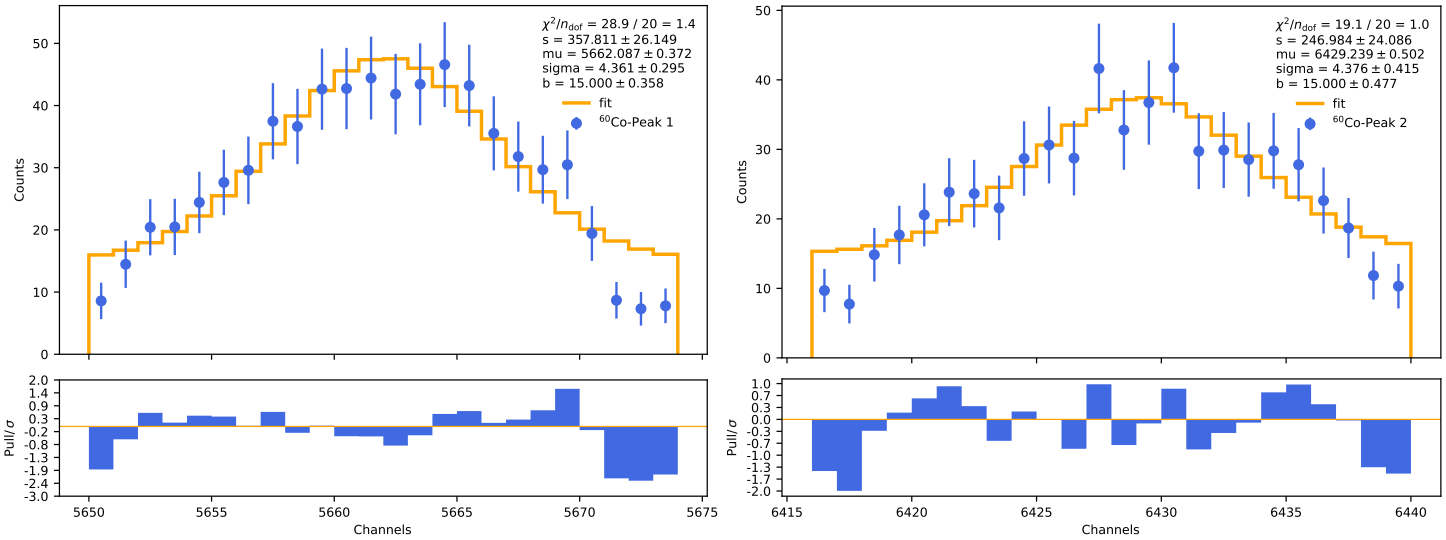

Figure 16: Fits of peaks of the ^{60}Co spectrum.

Table 4: Fit parameters of the two peaks of the ^{60}Co spectrum.

E/keV	s	b	μ	σ
1173.3856 ±0.0004	358 ±26	15.0 ±0.4	5662.1 ±0.4	4.4 ±0.3
1332.2939 ±0.0004	247 ±24	15.0 ±0.5	6429.2 ±0.5	4.4 ±0.4

To estimate the activity of the ^{60}Co source, Equation (9) is used. The full energy detection probabilities estimated in Section 4.2. Equation (9) is rearranged to be able to compute the probe activity:

$$Q = \frac{4\pi}{\Omega}\frac{N}{APt} \leftrightarrow A = \frac{4\pi}{\Omega}\frac{N}{QPt}. \tag{28}$$

The resulting activity and the values used are given in Table 5.

Table 5: Parameters and result of the activity calculation based on the two peaks of the ^{60}Co spectrum.

E/keV	A/Bq	N	P/%	t/s	Q
1173.3856 ±0.0004	995 ±138	358 ±26	99.85 ±0.03	4021	0.0074 ±0.0009
1332.2939 ±0.0004	771 ±118	247 ±24	99.9826 ±0.0006	4021	0.0066 ±0.0008

The averaged activity then results to

$$\bar{A} = (883.1 \pm 116.5)\,\text{Bq}. \tag{29}$$

4.5 Spectrum of an unknown source

A measurement of an unknown uranium source is conducted. The measured spectrum is displayed in Figure 17; the measurement time is $t = 2968\,\text{s}$.

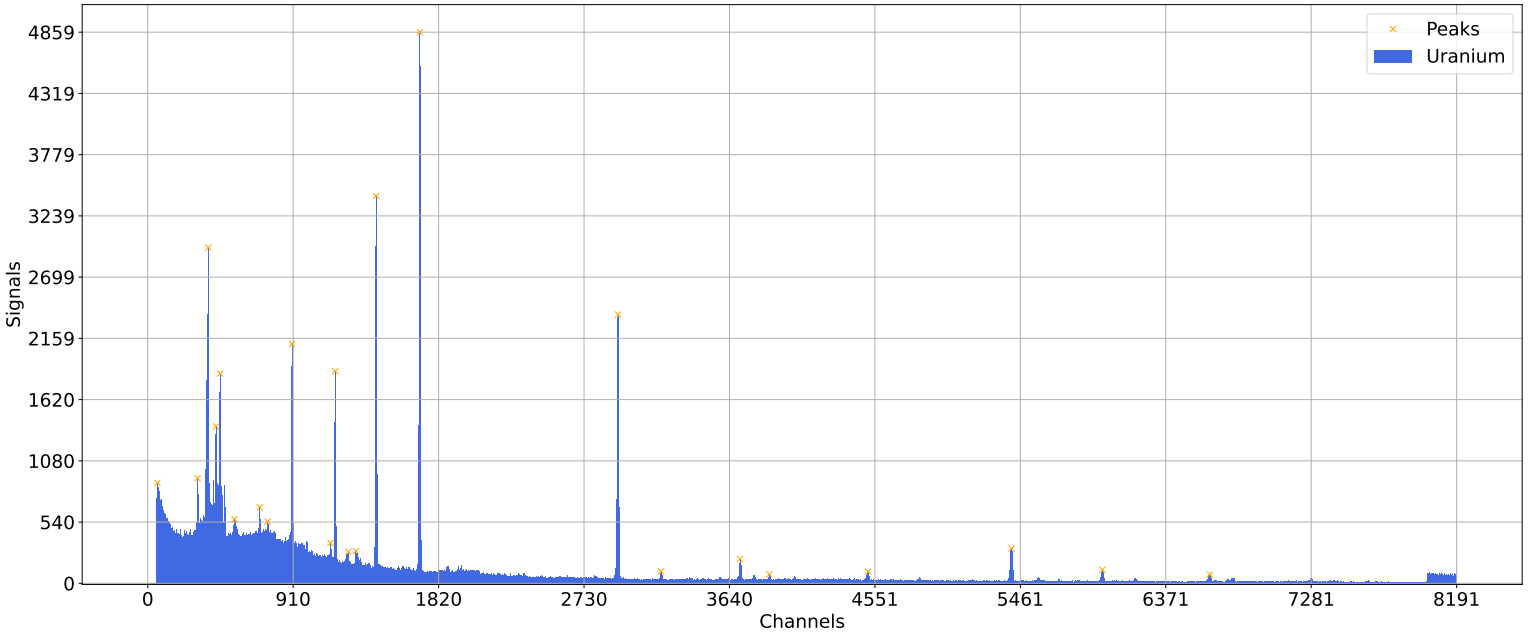

Figure 17: Spectrum of the uranium measurement.

The background measurement is displayed in Figure 18.

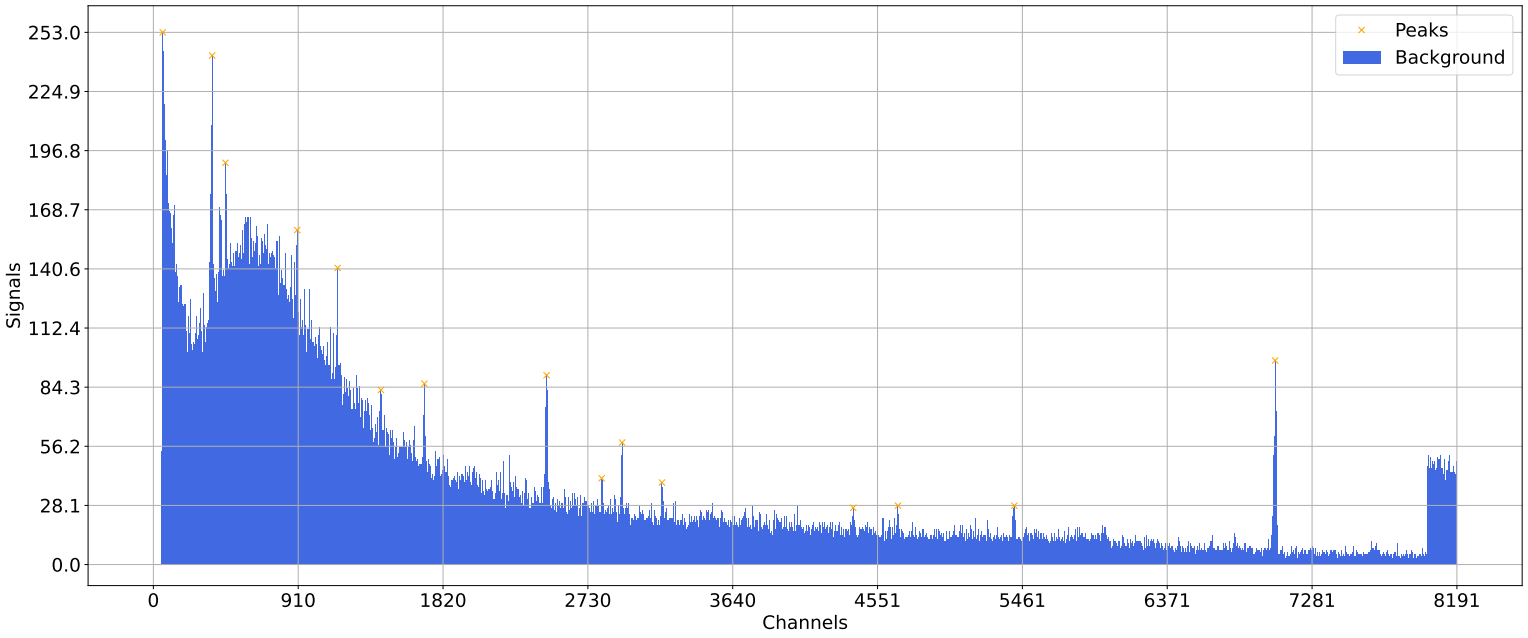

Figure 18: Spectrum of the background measurement.

Through comparing the peaks of both spectra, the ones which likely originate from the uranium probe can be identified. These peaks are shown in Figure 19.

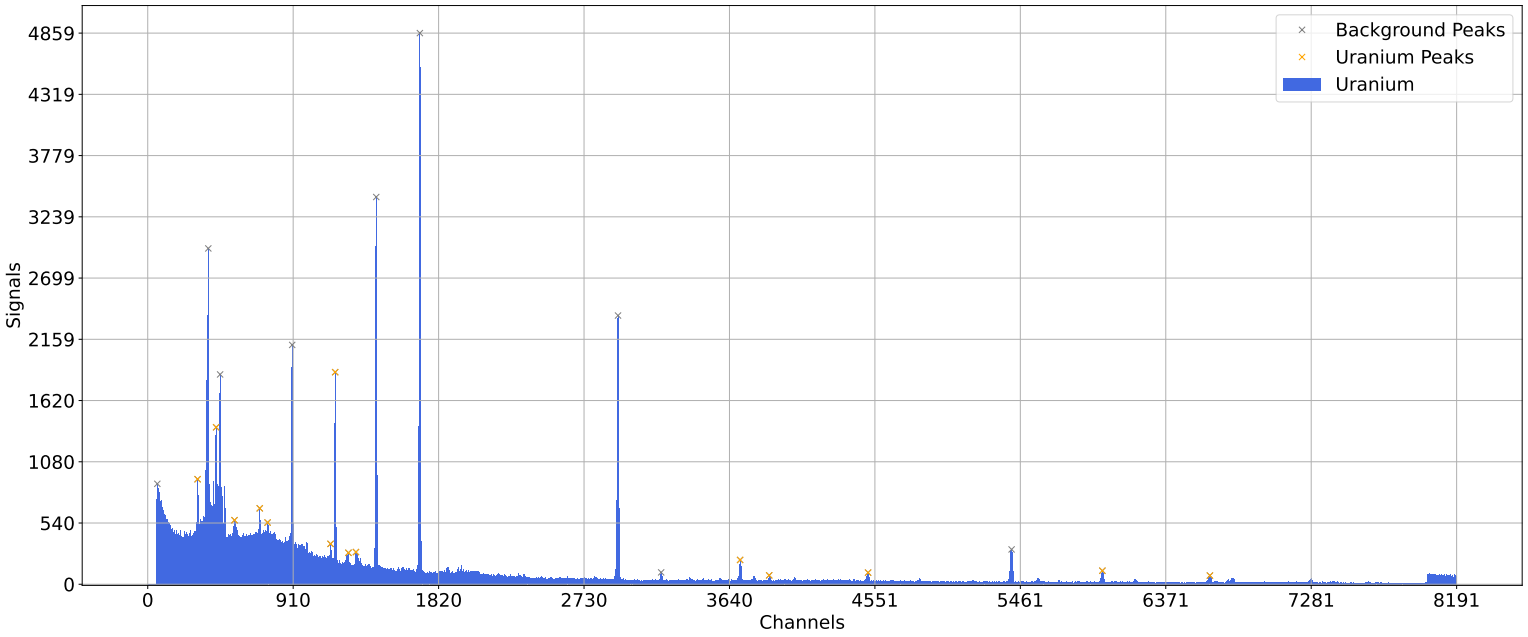

Figure 19: Spectrum of the uranium measurement, with background peaks removed.

The exact channels of the peaks of the uranium measurement and the background measurement are given in Table 6. A normal distribution is fitted to the remaining peaks to estimate the yield; the results are given in Figure 20.

Table 6: Channels of peaks in the background and uranium spectrum.

Index	C_{Ur}	C_{B}
0	60	59
1	312	-
2	379	370
3	428	-
4	453	453
5	543	-
6	701	-
7	750	-
8	904	904
9	1144	-
10	1173	-
11	1256	-
12	1303	-
13	1430	1430
14	1703	1703
15	2943	2946
16	3213	3196
17	3707	-
18	3889	-
19	4508	-
20	5406	5410
21	5974	-
22	6647	-

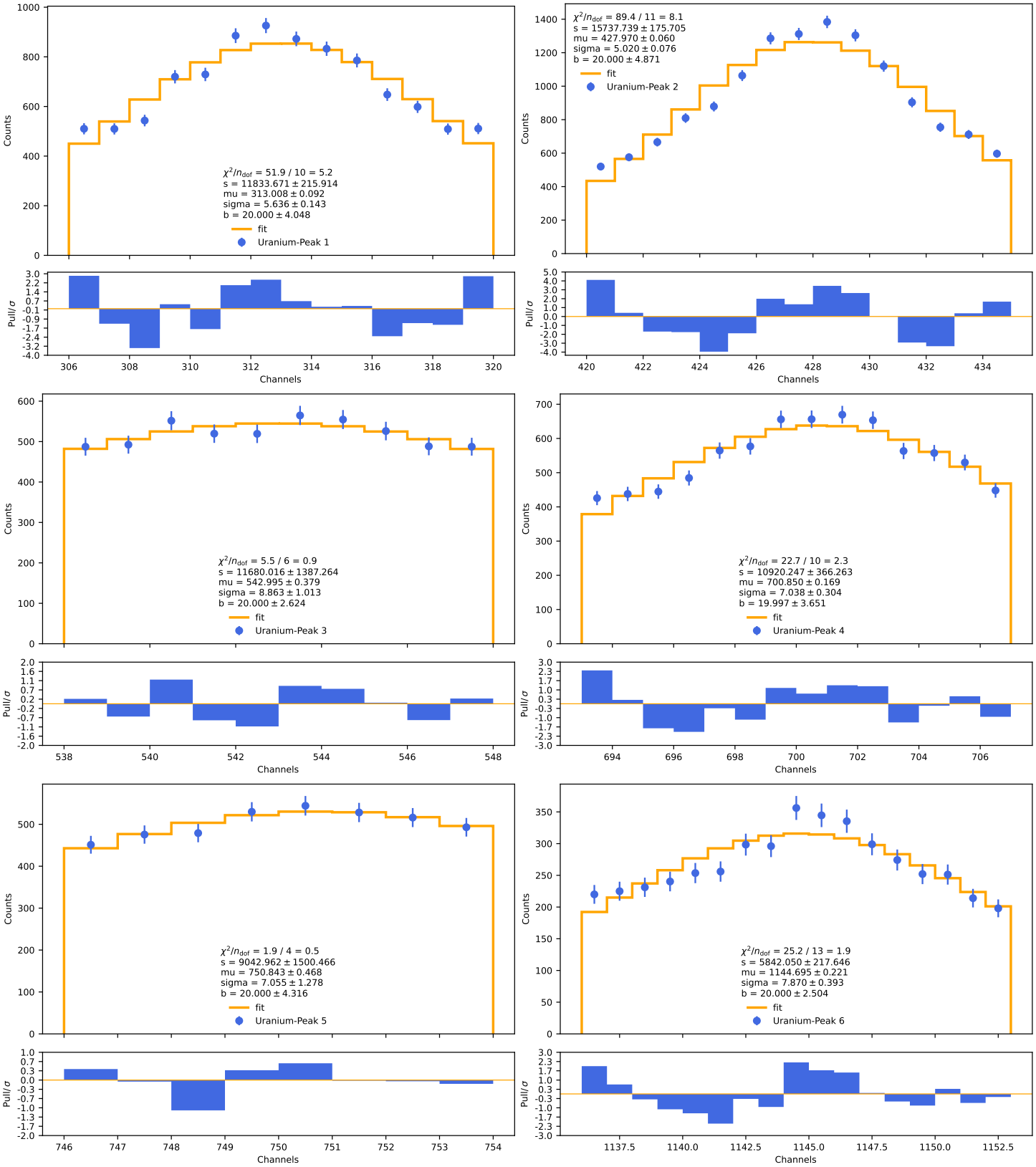

Figure 20: Fits of peaks of the peaks of the uranium spectrum.

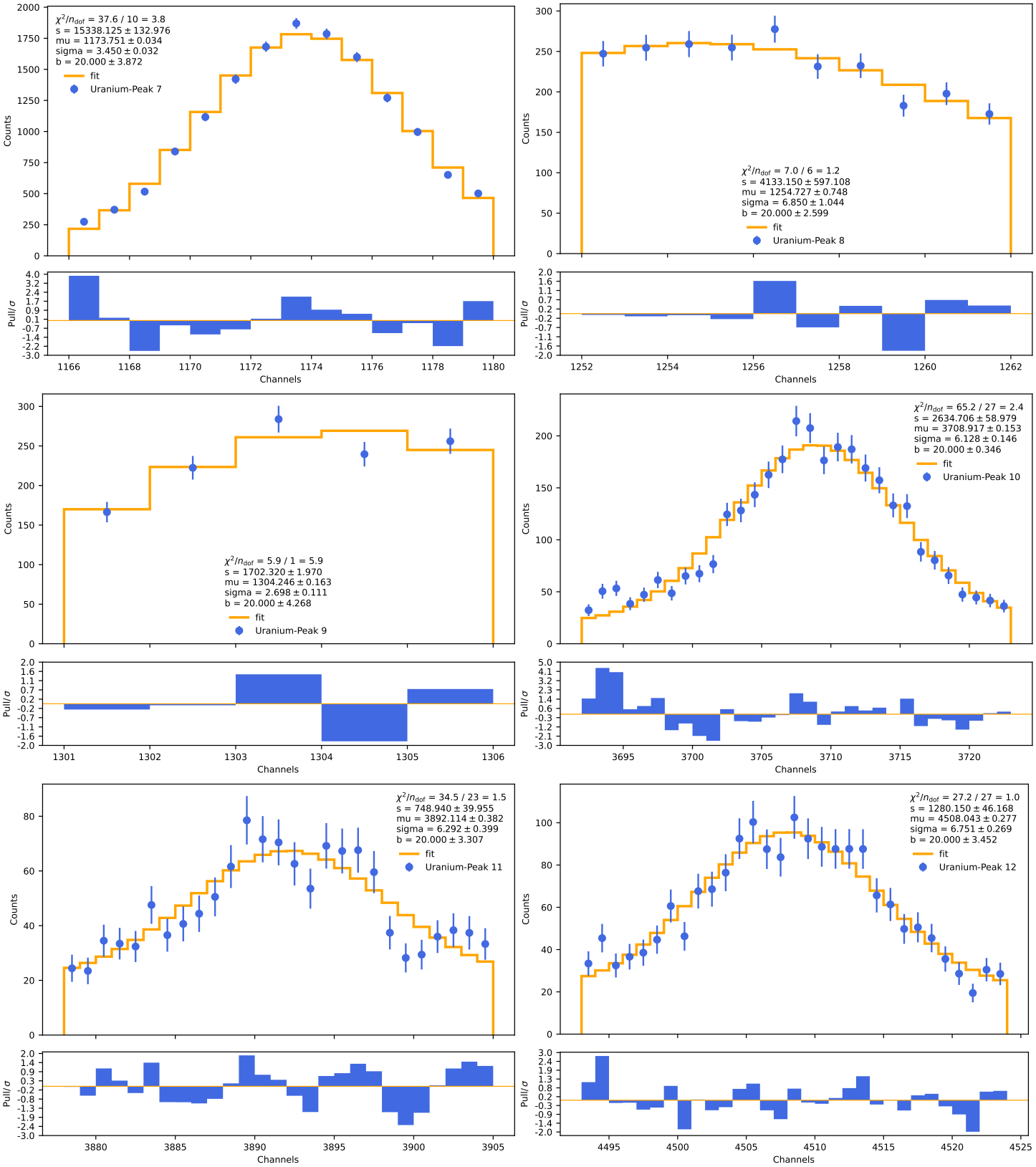

Figure 21: Fits of the peaks of the uranium spectrum.

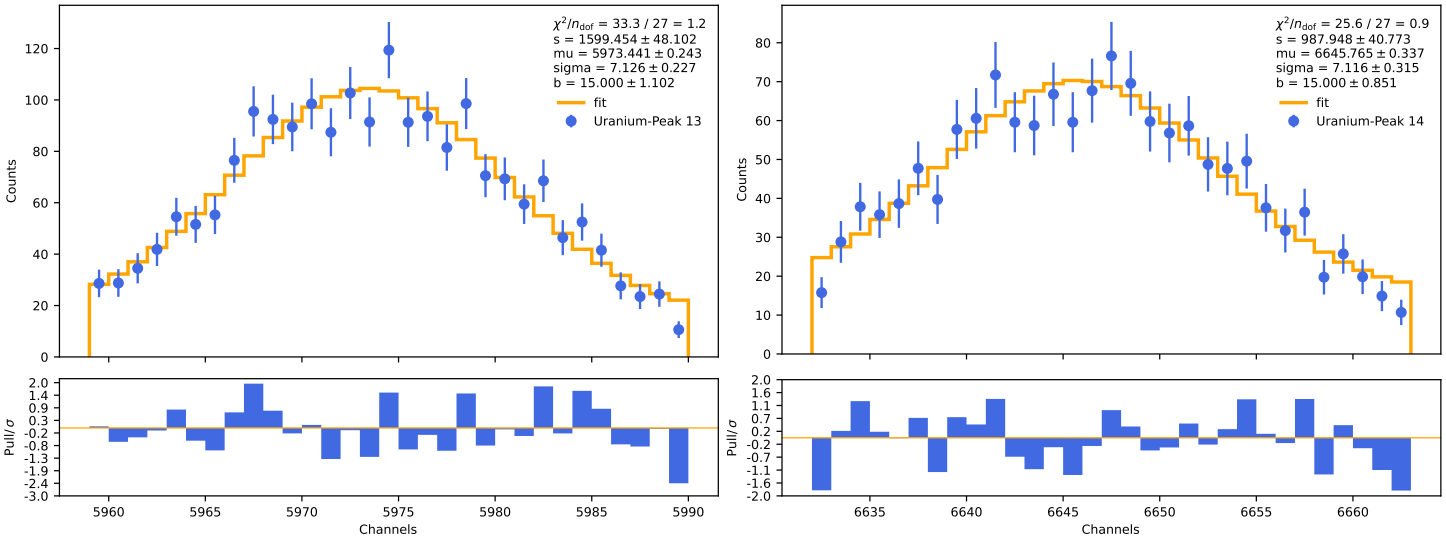

Figure 22: Fits of the peaks of the uranium spectrum.

The emission lines are matched to possible nuclides from the literature [1]. A possible matching is given in Table 7.

Table 7: Matching of peaks of the unknown uranium sources´ spectrum.

		^{233}U		^{226}Ra		^{214}Pb		^{214}Bi	
Index	Peak/keV	Peak/keV	P/%	Peak/keV	P/%	Peak/keV	P/%	Peak/keV	P/%
0	63.1025 ±0.0004	62.950 ±0.017	0.49	62.5 ±1.0	0.0116	62.5 ±1.0	0.0116	62.5 ±1.0	0.0116
1	87.1670 ±0.0004	87.385 ±0.016	0.271	-	-	-	-	-	-
2	111.0239 ±0.0004	111.517 ±0.018	0.313	-	-	-	-	-	-
3	143.8014 ±0.0004	144.627 ±0.042	0.00046	-	-	-	-	-	-
4	153.9665 ±0.0004	153.955 ±0.018	0.205	-	-	-	-	-	-
5	235.7026 ±0.0004	-	-	-	-	-	-	-	-
6	241.7187 ±0.0004	240.663 ±0.021	0.0117	-	-	-	-	-	-
7	258.9372 ±0.0004	-	-	258.87 ±0.03	0.5318	258.87 ±0.03	0.5318	-	-
8	268.6875 ±0.0004	-	-	-	-	-	-	268.8 ±0.2	0.0161
9	767.4021 ±0.0004	-	-	-	-	-	-	768.356 ±0.010	4.892
10	805.1583 ±0.0004	-	-	-	-	-	-	806.174 ±0.018	1.262
11	933.5711 ±0.0004	-	-	-	-	-	-	934.061 ±0.012	3.10
12	1237.6958 ±0.0004	-	-	-	-	-	-	1238.111 ±0.012	5.831
13	1377.3110 ±0.0004	-	-	-	-	-	-	1377.669 ±0.012	3.968

The unknown source likely consists of ^{233}U, ^{214}Bi and its daughter nuclides ^{226}Ra and ^{214}Pb, as these would inhibit all measured emission lines which could be attributed to the source. For each nuclide and peak the activity is calculated using the literature values given in Table 7. The resulting activitys are given in Table 8.

Table 8: Results of the activity calculation based on the aforementioned peaks in the measured spectrum, ordered by presumed nuclide.

Index	Peak/keV	$A(^{233}\mathrm{U})$/kBq	$A(^{226}\mathrm{Ra})$/kBq	$A(^{214}\mathrm{Pb})$/kBq	$A(^{214}\mathrm{Bi})$/kBq
0	63.1025 ±0.0004	63 ±6	-	-	-
1	87.1670 ±0.0004	202 ±19	-	-	-
2	111.0239 ±0.0004	162 ±25	-	-	-
3	143.8014 ±0.0004	130882 ±13486	-	-	-
4	153.9665 ±0.0004	51 ±5	-	-	-
5	235.7026 ±0.0004	-	-	-	-
6	241.7187 ±0.0004	11624 ±1190	-	-	-
7	258.9372 ±0.0004	-	73 ±13	-	-
8	268.6875 ±0.0004	-	-	-	1033 ±106
9	767.4021 ±0.0004	-	-	-	19.3 ±2.2
10	805.1583 ±0.0004	-	-	-	56 ±6
11	933.5711 ±0.0004	-	-	-	7.4 ±0.9
12	1237.6958 ±0.0004	-	-	-	8.68 ±1.06
13	1377.3110 ±0.0004	-	-	-	17.6 ±2.2

5 Conclusion

The detector calibration shows satisfactory results, which is important as all other results depend on the energy calculation. Therefore the low uncertainties of the fit parameters help to reduce uncertainties in the following computations. The result for the activity of the europium source is of the expected order. The full energy detection probability calculation follows the expected distribution, although the results deviate more for lower energies; however, this is expected as the detector sensitivity is better for higher energy values. The limiting factor in the analysis of the europium spectrum (as well as all subsequent spectrum analysis) is the rudimentary background estimation. The results could probably be improved by a significant amount if a background fit would be performed. A more sophisticated fit distribution for the peaks could be useful as well, as there are often slight asymmetries in the peaks which the normal distribution can not account for. Aside from these possible improvements, the caesium peak fits and calculation of the full and tenth width at half maximum seem plausible. The compton edge can only be roughly estimated; a longer measurement time should improve the contrast and result in more accurate values. The estimation of the compton continuum and the influence of the backscatter peak on it would both benefit greatly from performing additional fits of the backscatter peak and the background. The cobalt spectrum analysis shows (aside from the already mentioned shortcomings of the background estimation)

satisfactory results. The identification of the unknown source probably suffers the most by the not ideal background estimation; the matching of peaks of the measurement by comparing it to the background measurement could probably be improved. For some fits (e. g. Peak 9) the statistics are to low to perform a meaningful fit, resulting in compromised results. A longer measurement time could help mitigate this problem. However, the given nuclides seem to explain the measured spectrum reasonably well, but it remains unclear if there is another combination with higher emission probabilities, which are relatively low for some emission lines.

References

[1] Laboratoire National Henri Becquerel. *Library for gamma and alpha emissions*. 2004. URL: http://www.lnhb.fr/Laraweb/index.php (visited on 12/14/2023).

[2] Hans Dembinski and Piti Ongmongkolkul et al. "scikit-hep/iminuit". In: (Dec. 2020). DOI: 10.5281/zenodo.3949207. URL: https://doi.org/10.5281/zenodo.3949207.

[3] I-Yang Lee, M Deleplanque, and Kai Vetter. "Developments in large gamma-ray detector arrays". In: *Reports on Progress in Physics* 66 (May 2003), p. 1095. DOI: 10.1088/0034-4885/66/7/201.

[4] Laboratory for Nuclear Technologies. *Interaction of γ-rays with matter*. 2023. URL: https://www.fe.infn.it/radioactivity/educational/detection.html (visited on 11/14/2023).

[5] Hastings A. Smith and Marcia Lucas. "Gamma-Ray Detectors". In: 1997. URL: https://api.semanticscholar.org/CorpusID:19059674.

[6] Pauli Virtanen et al. "SciPy 1.0: Fundamental Algorithms for Scientific Computing in Python". In: *Nature Methods* 17 (2020), pp. 261–272. DOI: 10.1038/s41592-019-0686-2.